# Turbulence Energy and Intensity Spectra in a Baffled, Stirred Vessel

**W. J. KIM and F. S. MANNING**

*Carnegie Institute of Technology, Pittsburgh, Pennsylvania*

The radial components of the turbulence energy and intensity spectra within a stirred, baffled tank are measured with a transducer probe of the type developed by Eagleson et al. (9). The spectra are normalized because absolute levels of the intensity in these high intensity velocity fields cannot be measured with the present technique. Average velocities are also measured with Pitot and Prandtl tubes.

Range of measured energy and intensity spectra was 19 to 1,100 cycles/sec. The measured energy spectra show a $k^{-5/3}$-relation in the low wave number range where the wave number $k$ is less than 100 ft.$^{-1}$ and a $k^{-10/3}$-relation in the wave number range of 100 to 1,000 ft.$^{-1}$. This behavior is found regardless of impeller size, motor speed, and position in tank, in particular radial distance, indicating that the decay of energy spectra is self-preserving. Increasing the viscosity from 0.80 to 103 centipoises results in a progressively steeper slope in the high wave number range. The shape of the intensity spectra is the same as that of the concentration spectra measured by Manning (26, 27).

Although the use of a stirred, baffled tank as a mixing device in chemical industry is as old as the chemical industry itself, the technique of mixing in the tank has remained an art rather than a science. The extremely complex three-dimensional flow within the tank renders a theoretical treatment intractable.

There have been a number of phenomenological, or macroscopic, approaches in which the measurable quantities, such as power input per unit volume, rate of dissolution of a solute, etc., are used as the criteria of mixing efficiency (*25*).

Recently theoretical studies with turbulence theory as background have been conducted by Corrsin (*6*), who applied isotropic turbulence theory to an idealized turbulent mixer and derived the expression for the rate of decrease in concentration fluctuations in terms of the turbulence scale and the power input to the system. Corrsin (*7*) also considered an additional factor of chemical reaction in the mixing process and deduced rate equations for some statistical functions of the concentration of the reactant under highly idealized conditions. Theoretical work on other types of flow, for examples pipes (*3*) and wind tunnels, is not reviewed.

A rigorous theoretical treatment of the mixing problem coupled with turbulence theory is necessarily difficult and intractable, and therefore some simplifying assumptions along with the experimental determination of desired turbulence parameters are mandatory. Measurements of flow and turbulence characteristics in a stirred and baffled tank are still in an early stage of development. The main difficulty that has prevented measurement of the turbulence parameters in a stirred tank is the fact that this turbulence is a liquid phase type of abnormally high relative intensity. While the hot-wire anemometer plays an indispensable role in the measurements of gas turbulence parameters, it does not give a satisfactory result in case of liquid turbulence because of its weak mechanical strength and its sensitivity to the surface contamination of the hot wire. The hot-film anemometer with an improved mechanical strength has been introduced by Ling and Hubbard (*25*). It has been used by Cohen (*5*) to measure the Reynolds stresses and by Lee (*22*) to measure the energy spectrum in a water pipe flow. However enough data have not been collected to determine the reliability of the hot-film anemometer.

A light technique was used by Sachs and Rushton (*31*) to measure the average velocity distribution in a stirred and baffled tank. Cutter (*8*) calculated Eulerian correlation coefficients and also Eulerian scales of turbulence of water in a fully baffled, stirred tank from the photographic data obtained by the light technique. Although the turbulence energy spectrum can be calculated, at least theoretically, from the corresponding correlation function as its Fourier transform, the reliability of this method cannot be estimated, and hence the direct measurement of energy spectrum is desirable. However the light technique cannot be used to measure the energy spectrum directly.

Recently Ippen et al. (*12, 13*) developed a transducer probe which is sensitive to pressure fluctuations. This probe has been improved by Perkins, Eagleson, and Huval (*30, 9*), who used it to measure the energy spectrum behind a flat plate in the water tunnel.

The purpose of this work is to measure the turbulence energy spectra in a stirred and fully baffled tank with the transducer probe and to study the effects of impeller size and of liquid viscosity on the shape of the spectrum functions. Also the theoretical predictions of turbulence energy spectrum were reviewed and compared with the experimental results.

## THEORY

In this section theoretically predicted energy spectra are discussed briefly.

The dynamic equation of energy spectrum can be obtained by taking the Fourier transform of the Karman-Howarth equation (*15*):

$$\frac{\partial}{\partial t} E(k, t) = W(k, t) - 2\nu k^2 E(k, t) \qquad (1)$$

However the above equation is indeterminate owing to the unknown behavior of $W$. There have been two approaches to get around this difficulty. The first method discards Equation (1) and draws some conclusions about the functional form of $E$ from the similarity hypothesis; the second assumes an explicit functional form for $W$ and solves Equation (1). These methods indicate that the whole energy spectrum range may be conveniently divided into four ranges: large eddies range, energy containing eddies range, and universal equilibrium range which is

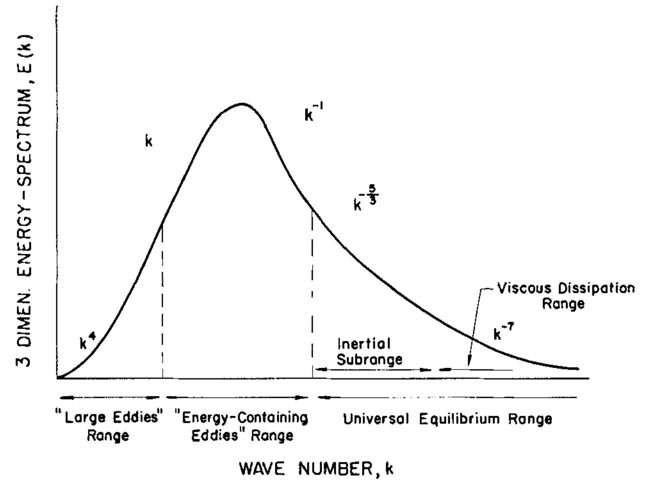

Fig. 1. Theoretical spectrum.

further divided into inertial subrange and viscous dissipation subrange. Using the first approach Batchelor (*1, 2*) and Lin (*23, 24*) showed that $E(k) \sim k^4$ in the large eddies range. Von Karman and Lin (*16*) postulated the existence of a parameter $D_o$ which characterizes the energy transfer mechanism and showed by dimensional analysis that $E(k) \sim D_o^2 k$ in the subrange where $E$ depends only on $D_o$. In 1941 Kolmogoroff (*18, 19, 20*) introduced the important concepts of local isotropy and the two similarity hypotheses, from which he derived that $E(k) \sim k^{-5/3}$ in the inertial subrange of the universal equilibrium range. This negative five-thirds power law has also been obtained independently by von Weizsacker (*33*) and Onsager (*29*). The second approach has been used by Tchen (*32*) who divided the equilibrium range into three subranges and showed, by a harmonic analysis, that $E(k)$ is proportional to $k^{-1}$, $k^{-5/3}$, and $k^{-7}$, respectively, in the three subranges. In the viscous dissipation subrange the $k^{-7}$-relation was obtained by Heisenberg (*10, 11*) who assumed an explicit functional form for the energy transfer function. Similar results have been obtained by Chandrasekhar (*4*), Obukhoff (*28*), Kovasznay (*21*), and von Karman (*14*). These theoretical results are summarized in Figure 1.

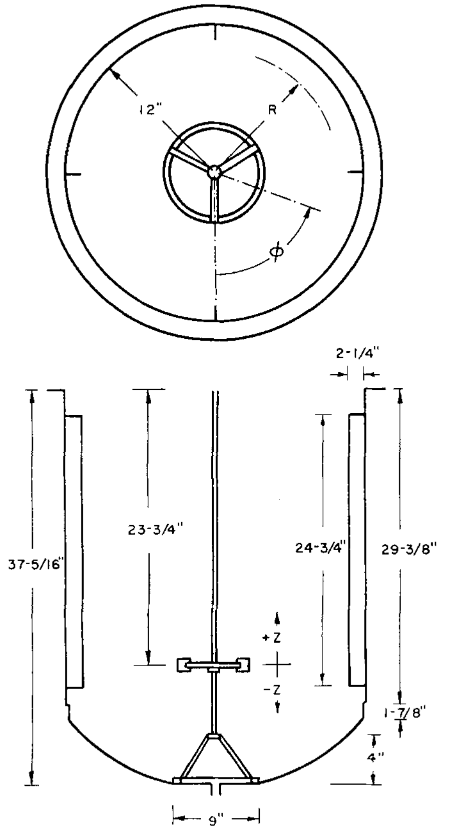

Fig. 2. Stirred tank.

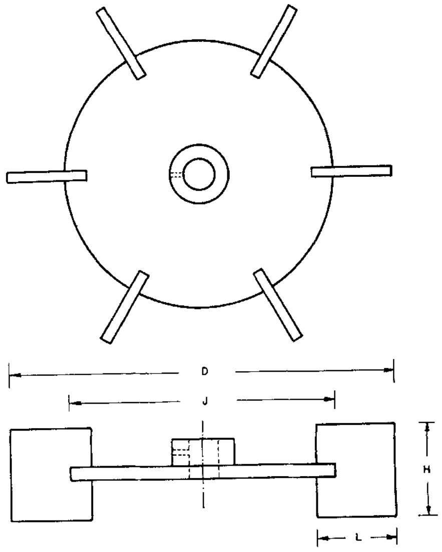

| IMPELLER | INCHES | | | |
|---|---|---|---|---|
| | D | J | L | H |
| A | 5 | 3-3/8 | 1-1/4 | 1 |
| B | 6 | 4 | 1-1/2 | 1-3/16 |
| C | 7 | 4-3/4 | 1-11/16 | 1-3/8 |

Fig. 3. Schematic diagram and dimensions of impeller.

## EXPERIMENTAL

Experimental equipment, procedure, data processing, and results are now described very briefly in this order. Further details are available elsewhere (*17*).

### Equipment

The equipment consists of a baffled, stirred vessel, Pitot and Prandtl tubes, a barium titanate transducer probe of the type developed by Eagleson, et al. (*9*), and attendant electronic gear.

The stirred and baffled tank is shown in Figure 2. The upper end of the impeller shaft is connected to a horizontally mounted 2-hp. motor by means of a flexible shaft. Rotational speed, continuously variable from 100 to 1,675 rev./min., was measured with a hand tachometer. The tank is traversed with a holding mechanism sliding back and forth in a slotted arm. The arm is hinged at the center of the tank, thus permitting angular rotation. Turbine type of impellers of three different sizes, as shown in Figure 3, were used.

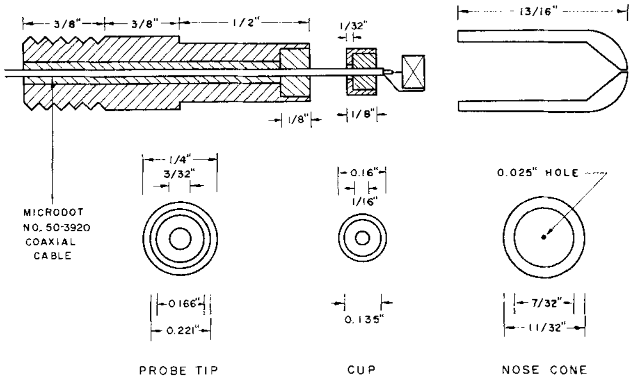

Fig. 4. Design of transducer probe tip.

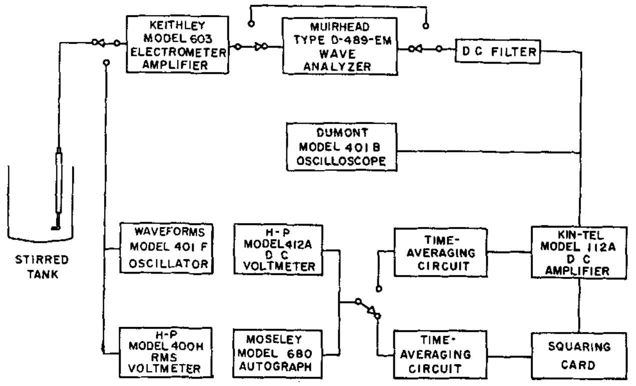

Fig. 5. Electronic circuit.

The Pitot tube is made of a stainless steel tubing, ¼ and 0.063 in. in O.D. and I.D., respectively. The tube is hook-shaped so that the position of the pressure port remains unchanged with respect to the rotation of the tube stem. This configuration compensates for the error resulting from the liquid surface distortion due to the very presence of the probe in static pressure measurements.

The Prandtl tube is a ¼-in. stainless steel tubing with a fluid calming section at the tip of the tubing. The calming section consists of two 1¼-in. diameter disks, one of which has a hole in the middle and is welded vertically onto the tube tip. The other disk is fixed parallel to and 1/32 in. apart from the first one by means of three screws. Pressure is measured with an open end U tube manometer with water as the manometric liquid.

In the transducer probe a circular, disk shaped barium titanate ceramic, 0.125 in. in diameter and 0.100 in. thick, was used as the pressure sensor. Both faces of the crystal are silvered, and they serve as electrodes. A tiny wire is carefully soldered onto each electrode, and then finally the whole crystal is coated with protective film. Figure 4 shows the design of the transducer probe tip. The crystal sits in a plastic cup which plugs into a stainless steel probe tip. The cup is fastened to the probe tip with the aid of a small amount of epoxy resin. In order to achieve a point measurement, a nose cone with a 0.025-in. hole is filled with water and then fitted over the probe tip. In practice considerable care must be exercised to prevent any trapped air in the nose cone. The filling operation was always performed under water. A teflon nose cone proved satisfactory because it fitted onto the tip very smoothly and is capable of keeping the fit air tight. The flexibility of the teflon apparently did not unduly spread the area measured.

The electronic circuit consists of an electrometer amplifier, a wave analyzer system, a squaring and time averaging circuit, a voltmeter, a recorder, and other auxiliary units. The schematic diagram is shown in Figure 5. Detailed circuit diagrams and equipment characteristics are given elsewhere (*17*).

### Procedure

An open end U tube manometer was used to measure the radial average velocities. The pitot tube was placed in position and connected to the manometer by means of Tygon tubing. The fluctuation in the U tube manometer was cut down by pinching the Tygon tubing with a small clamp. Each reading was taken when the fluctuation stayed ± 3 mm. for at least 5 min. The same procedure was used to measure the static pressure with the Prandtl tube.

Measurements of energy spectrum curves were made in four steps: measurements of total output for Fourier component of turbulence intensity, corresponding noise output, total output for turbulence intensity, and corresponding noise output. In the first and third steps the nose cone with a hole is used, while in the second and fourth steps the nose cone without a hole is employed. In the first step the transducer probe without the teflon nose cone was placed in position, the nose cone with a hole was filled with water and carefully examined to ensure the absence of trapped air bubbles, and then it was put onto the transducer probe tip under water. The wave analyzer was set to a desired frequency and gain. The time constant of the squaring and time averaging circuit was slowly increased to a value at which the output fluctuation remains within ± 2% of the output level. Readings were taken from the voltmeter when the output stayed steady for ten minutes. The same procedure was used in the second step except that the nose cone with a hole was now replaced by the one without a hole. In the third and fourth steps the wave analyzer was bypassed.

The scope of energy spectrum measurements was:

| | |
|---|---|
| Frequency range: | 19 to 1,100 cycles/sec. |
| Fluid viscosity: | 0.80, 10.60, and 103 centipoises |
| Impeller diameter: | 5, 6, and 7 in. |
| Motor speed: | 200, 400, 600, and 800 rev./min. |
| Vertical distance, $Z$: | −⅝, 0, +⅝ in. |
| Longitude, $\phi$: | 0, 30, and 60 deg. |
| Radial distance, $R$: | 4, 5, and 6 in. |

## DATA PROCESSING

Average velocity and spectra data are treated separately.

Average velocities are calculated with the well-known formula

$$\overline{U}_1 = \sqrt{2g_c\Delta H} \tag{2}$$

Turbulence intensity $\sqrt{\overline{u_1^2}}$ is shown by Ippen et al. (*13*) to be related to transducer output $G_s$ as follows:

$$\sqrt{\overline{u_1^2}} = \frac{g_c\sqrt{\overline{G_s^2}}}{K\overline{U}_1} \tag{3}$$

Intensity spectra as a function of frequency $F(n)$ and as a function of wave number $E_1^o(k)$ are defined by

$$F(n) = \frac{\sqrt{\overline{u_1^2}(n)}}{\sqrt{\overline{u_1^2}}} \tag{4}$$

and

$$E_1^o(k) = \frac{\overline{U}_1}{2\pi}F(n) \tag{5}$$

Combining Equations (3) and (4) one obtains

$$F(n) = \frac{\sqrt{\overline{G_s^2}(n)}}{\sqrt{\overline{G_s^2}}} \tag{6}$$

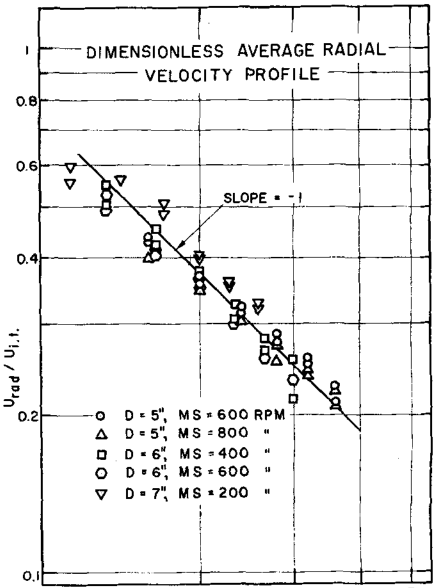

Fig. 6. Dimensionless average radial velocity profile.

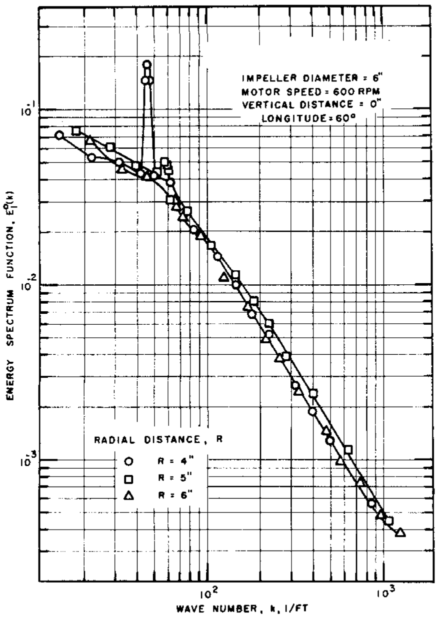

Fig. 7. Radial intensity spectrum.

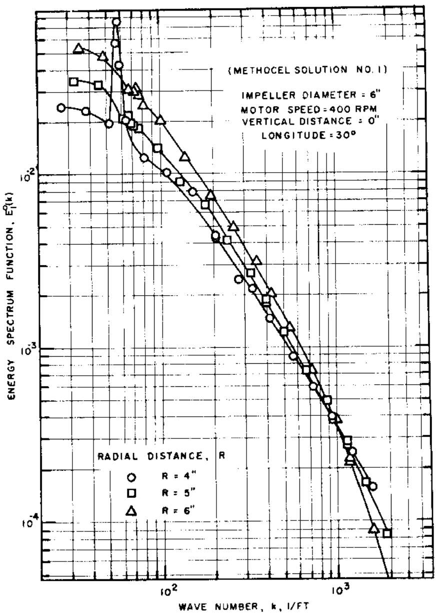

Fig. 8. Radial intensity spectrum.

The root-mean-square value of amplified true turbulence signal $\sqrt{\overline{V^2}_{t.s.}}$ is obtained as follows (*17, 27*):

$$\sqrt{\overline{V^2}_{t.s.}} = \sqrt{\overline{V^2}_{\text{total}} - \overline{V^2}_{\text{noise}}} \tag{7}$$

Hence the root-mean-square value of the transducer output due to turbulence $G_s$ is

$$\sqrt{\overline{G_s{}^2}} = \frac{\sqrt{\overline{V^2}_{\text{total}} - \overline{V^2}_{\text{noise}}}}{(E.G.)\,(W.A.G.)\,(B.P.F.)} \tag{8}$$

Combining Equations (5), (6), and (8) one gets

$$E_1{}^o(k) = \frac{\overline{U}_1}{2\pi} \left\{ \frac{\left\{ \dfrac{\sqrt{\overline{V^2}_{\text{total}}\,(k) - \overline{V^2}_{\text{noise}}\,(k)}}{(E.G.)\,(W.A.G.)\,(B.P.F.)} \right\}}{\left\{ \dfrac{\sqrt{\overline{V^2}_{\text{total}} - \overline{V^2}_{\text{noise}}}}{(E.G.)} \right\}} \right\} \tag{9}$$

The corresponding energy spectra $G(n)$ and $E_1(k)$ are defined as

$$G(n) = \frac{\overline{u_1{}^2(n)}}{\overline{u_1{}^2}} \tag{10}$$

and

$$E_1(k) = \frac{\overline{U}_1}{2\pi} G(n) \tag{11}$$

Comparison of Equations (4), (5), (10), and (11) shows

$$E_1(k) = \frac{2\pi}{\overline{U}_1} (E_1{}^o\,(k))^2 \tag{12}$$

Typical average velocity data are shown in Figure 6 and intensity spectrum data in Figures 7 to 9. The original data are given elsewhere (*17*).

## DISCUSSION

Since water is practically incompressible, the assumption of axisymmetrical flow at the center of the impeller stream requires that

$$2\pi R.\overline{U}_{\text{rad}} = K_1 = \text{const} \tag{13}$$

or

$$\left(\frac{2R}{D}\right) \left\{ \frac{\overline{U}_{\text{rad}}}{U_{i.t.}} \right\} = K_2 = \text{const} \tag{14}$$

Taking logarithms of both sides of Equation (14) one gets

$$\ln \left\{ \frac{\overline{U}_{\text{rad}}}{U_{i.t.}} \right\} = \ln K_2 - \ln \frac{2R}{D} \tag{15}$$

Therefore the plot of $\overline{U}_{\text{rad}}/U_{i.t.}$ vs. $2R/D$ on a log-log scale should give a straight line of slope $-1$. This plot has been prepared for five different cases. As shown in Figure 6 the data points scatter around the straight line of slope $-1$, and hence the assumption of axisymmetric flow is considered satisfied. Figure 6 also shows that the radial velocity is proportional to the impeller tip velocity at various distances. Since impeller tip velocities vary between 6 to 15 ft./sec., absolute values of the mean veloc-

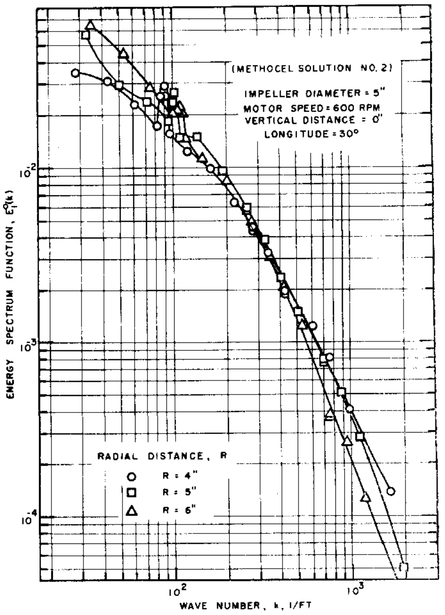

Fig. 9. Radial intensity spectrum.

ities cover the range of 1 to 9 ft./sec. This is in agreement with the results obtained by Sachs and Rushton (*31*) and Cutter (*8*).

The present intensity spectra cover a frequency range of 20 to 1,100 cycles/sec. A most important conclusion is immediately apparent. All spectrum curves exhibit a remarkable constancy; in fact their shape is practically unaffected by impeller size, motor speed, and probe position within the impeller stream. Manning and Wilhelm (*27*) reported a similar constancy for concentration spectra. In view of this spectra independence of the usual mixing study variables it is difficult to see how spectral data can be used to explain the effect that these mixing variables have on chemical reaction yields and selectivity. Additional data, for example absolute values of pressure, concentration, and velocity intensities, are obviously needed.

When frequency is converted to wave number, the turbulence intensity spectra extend over the region where $E_1{}^o(k) \sim k^{-5/3}$ as shown in Figure 7. This means that the corresponding energy spectrum $E_1(k)$ is proportional to $k^{-10/3}$. Spectral curves also show a slight decrease in the slope in the wave number range of less than 100 and approach a slope of $-5/6$, while they have the expected peaks at the wave number corresponding to the turbulence-generating frequency [defined as (motor speed, rev./min.) (number of impeller blades)/60] when the turbulence generating frequency is not greater than 60. The peaks however decay rapidly and become barely noticeable at $R = 5$ in. This behavior is in marked contrast to the general shape of intensity spectrum, which remains virtually unchanged within the measured range of radial distance. When the turbulence generating frequency is 80, no peak is observed even at $R = 4$ in., thus indicating that a fluctuation of higher frequency decays faster.

In the case of methocel solution No. 1 ($\mu = 10.6$ centipoises) the range where $E_1{}^o(k) \sim k^{-5/3}$ is observed in the wave number range of 300 to 1,500 at $R = 4$ in., as shown in Figure 8. At $R = 5$ in. the range shifts to the wave number range of 200 to 800, while in the higher wave number range the spectrum curve has a steeper slope. At $R = 6$ in. the range where $E_1{}^o(k) \sim k^{-5/3}$ is completely missing, and the spectrum curve has an even steeper slope.

In the case of methocel solution No. 2 ($\mu = 103$ centipoises) the $k^{-5/3}$-relation is not obtained at any radial distance, as shown in Figure 9, and the slope of the spectrum curves become steeper as the radial distance is increased. The slope seems to approach Heisenberg's negative seventh power law range, but no conclusion can be drawn from this study because the measurements of still higher frequency portions of spectrum curves were impossible because of the low fundamental natural frequency of the transducer probe. The fact that the slope of the spectrum curves gets steeper at higher viscosities indicates that the increase in viscosity results in the faster decay of smaller eddies.

Attempts were made to measure average radial velocities and spectrum curves outside the impeller stream, but reproducible results could not be obtained. One possible explanation for this difficulty may be due to the fact that the flow condition is not steady, and hence the mean velocity obtained, in practice, by averaging over a finite time interval may change. If this is the case, no reproducible spectrum measurements can be expected because the output of the transducer probe is related to the average velocity, as shown in Equation (9).

## ACKNOWLEDGMENT

The authors gratefully acknowledge the generous support of the National Science Foundation in sponsoring this project.

## NOTATION

$B.P.F.$ = band pass factor of wave analyzer
$D$ = impeller diameter, in.
$D_o$ = parameter characterizing energy transfer mechanism, as postulated by Lin
$E$ = Heisenberg's energy spectrum
$E.G.$ = electrometer gain
$E_1(k)$ = one-dimensional energy spectrum as a function of $k$
$E_1{}^o(k)$ = one-dimensional intensity spectrum as a function of $k$
$F(n)$ = one-dimensional intensity spectrum as a function of $n$
$g_c$ = dimension conversion factor = 32.174 (lb. mass) (ft.)/(lb. force) (sec.$^2$)
$G(n)$ = one-dimensional energy spectrum as a function of $n$
$G_s$ = transducer output in volts
$\Delta H$ = impact head in feet of fluid
$k$ = absolute value of wave number vector $k$
$K$ = calibration constant
$K_1$ = constant used in Equation (13)
$K_2$ = constant used in Equation (14)
$n$ = frequency
$R$ = radial distance measured from the center of stirred tank
$t$ = time
$u_1$ = fluctuating velocity component in the 1 direction
$\overline{U}_1$ = average velocity component in the 1 direction
$\overline{U}_{i.t.}$ = impeller tip velocity, $\overline{U}_{i.t.} = \pi$ $D$. (rev./min.)
$\overline{U}_{\text{rad}}$ = average radial velocity
$V_{\text{noise}}$ = signal fed to the squaring and time averaging circuit when the probe tip is fitted with the nose cone without a hole, v.
$V_{\text{total}}$ = signal fed to the squaring and time averaging circuit when the probe tip is fitted with the nose cone with a hole, v.
$V_{t.s.}$ = true turbulence signal fed to the squaring and time-averaging circuit, v.
$W$ = energy transfer function
$W.A.G.$ = wave analyzer gain
$Z$ = vertical distance, as shown in Figure 1
$\mu$ = viscosity
$\nu$ = kinematic viscosity
$\phi$ = longitude, deg., as shown in Figure 1

## LITERATURE CITED

1. Batchelor, G. K., *Proc. Camb. Phil. Soc.*, **43**, 533 (1947).
2. ———, *Proc. Roy. Soc.* (*London*), **A195**, 513 (1949).
3. Beek, J., Jr., and R. S. Miller, *Chem. Eng. Progr., Symposium Series*, **55**, 23 (1959).
4. Chandrasekhar, S., *Proc. Roy. Soc.* (*London*), **A200**, 20 (1949).
5. Cohen, M. F., M.S. thesis, The Ohio State University, Columbus, Ohio (1962).
6. Corrsin, S., *A.I.Ch.E. Journal*, 3, 329 (1957).
7. ———, *The Physics of Fluids*, 1, 42 (1958).
8. Cutter, L. A., Eng. Sci. D. thesis, Columbia University, New York, New York (1960).
9. Eagleson, P. S., D. J. Huval, and F. E. Perkins, *Mass. Inst. Technol. Hydrodynamics Lab., Tech. Rept. No. 46* (1961).
10. Heisenberg, W., *Z. fur Phys.*, **124**, 628 (1948).
11. ———, *Proc. Roy Soc.*. (*London*), **A195**, 402 (1948).
12. Ippen, A. T., and F. Raichlen, *Proc. ASCE Journal*, Hydraulics Division HY5, 1392 (1957).
13. ———, R. S. Tankin, and F. Raichlen, *Mass. Inst. Technol. Hydrodynamics Lab., Tech. Rept. No.* 20 (1955).
14. von Karman, T., *Proc. Natl. Acad. Sci.* (*U.S.A.*), 34, 530 (1948).
15. ———, and L. Howarth, *Proc. Roy. Soc.* (*London*), **A164**, 192 (1938).

16. ———, and C. C. Lin, *Rev. Modern Phys.*, **21**, 516 (1949).
17. Kim, W. J., Ph.D. thesis, Carnegie Institute of Technology, Pittsburgh, Pennsylvania (1964).
18. Kolmogoroff, A. N., *Comptes rendus (Doklady) de l'Academie des sciences de l'U. R. S. S.*, **30**, 301 (1941).
19. *Ibid.*, **31**, 538 (1941).
20. *Ibid.*, **32**, 538 (1941).
21. Kovasznay, L. S. G., *J. Aeronaut. Sci.*, **15**, 745 (1948).
22. Lee, J., Ph.D. thesis, The Ohio State University, Columbus, Ohio (1962).
23. Lin, C. C., *First Symp. Appl. Math.*, Am. Math. Soc. (1947).
24. ———, "Proc. Seventh Int. Congr. Appl. Math., London," Vol. 2, Part 1 (1948).
25. Ling, S. C., and P. J. Hubbard, *J. Aeronaut. Sci.*, **23**, 890 (1956).
26. Manning, F. S., Ph.D. thesis, Princeton University, Princeton, New Jersey (1959).
27. ———, and R. H. Wilhelm, *A.I.Ch.E. Journal*, **9**, 12 (1963).
28. Obukhoff, A. M., *Comptes rendus (Doklady) de l'Academie des sciences de l'U. R. S. S.*, **32**, 19 (1941).
29. Onsager, L., *Phys. Rev.*, **68**, 286 (1945).
30. Perkins, F. E., and P. S. Eagleson, *Mass. Inst. Technol. Hydrodynamics Lab., Tech. Note No. 5*, (1959).
31. Sachs, J. P., and J. H. Rushton, *Chem. Eng. Progr.*, **50**, 597 (1954).
32. Tchen, C. M., *J. Res., Natl. Bur. Standards*, **50**, *No. 1*, p. 51 (1953).
33. von Weizsacker, C. F., *Z. fur Phys.*, **124**, 614 (1948).

*Manuscript received October 14, 1963; revision received March 16, 1964; paper accepted March 18, 1964.*

---

# Thickness Distribution in a Sheet Formed by Impinging Jets

**DAVID HASSON and RALPH E. PECK**

**Technion-Israel Institute of Technology, Haifa, Israel**

The impinging jets atomizer possesses certain advantages as a spraying device in prime movers, particularly for propellant injection in liquid rocket combustors (*1, 2*). As in other spraying devices the drop size characteristics are closely related to the thickness of the spray sheet prior to breakup. Study of the thickness distribution in the sheet formed by impinging jets is also of importance for the design of fan spray nozzles, which operate on a closely similar principle (*3*).

Though several attempts (*4, 5, 6*) have been made to analyze the thickness distribution in the sheet formed by impinging jets, no satisfactory solution to this problem has hitherto been available. This paper provides the first analytical solution fitting all experimental data reported in the literature.

## STREAMLINE PATTERN OF FLOW

Consider two cylindrical and equal jets of radius $R$ flowing at equal velocity $v_0$ but in opposite directions (Figure 1). If the two jets collide obliquely at a total included angle of $2\theta$, it is found that the liquid spreads into a flat sheet flowing in a plane perpendicular to that containing the axes of the two jets.

The flow around the sheet is uneven, the flux being largest in the forward flow direction and smallest in the

---

Ralph E. Peck is at the Illinois Institute of Technology, Chicago, Illinois.